Concentric transmon qubit featuring fast tunability and an anisotropic magnetic dipole moment

Jochen Braumüller,[1,a)] Martin Sandberg,[2] Michael R. Vissers,[2] Andre Schneider,[1] Steffen Schlör,[1] Lukas Grünhaupt,[1] Hannes Rotzinger,[1] Michael Marthaler,[3] Alexander Lukashenko,[1] Amadeus Dieter,[1] Alexey V. Ustinov,[1,4] Martin Weides,[1,5] and David P. Pappas[2]

[1]*Physikalisches Institut, Karlsruhe Institute of Technology, 76131 Karlsruhe, Germany*
[2]*National Institute of Standards and Technology, Boulder, Colorado 80305, USA*
[3]*Institut für Theoretische Festkörperphysik, Karlsruhe Institute of Technology, 76131 Karlsruhe, Germany*
[4]*National University of Science and Technology MISIS, Moscow 119049, Russia*
[5]*Physikalisches Institut, Johannes Gutenberg University Mainz, 55128 Mainz, Germany*

(Received 13 October 2015; accepted 7 January 2016; published online 21 January 2016)

We present a planar qubit design based on a superconducting circuit that we call concentric transmon. While employing a straightforward fabrication process using Al evaporation and lift-off lithography, we observe qubit lifetimes and coherence times in the order of 10 μs. We systematically characterize loss channels such as incoherent dielectric loss, Purcell decay and radiative losses. The implementation of a gradiometric SQUID loop allows for a fast tuning of the qubit transition frequency and therefore for full tomographic control of the quantum circuit. Due to the large loop size, the presented qubit architecture features a strongly increased magnetic dipole moment as compared to conventional transmon designs. This renders the concentric transmon a promising candidate to establish a site-selective passive direct $\hat{Z}$ coupling between neighboring qubits, being a pending quest in the field of quantum simulation. © *2016 AIP Publishing LLC*.
[http://dx.doi.org/10.1063/1.4940230]

Quantum bits based on superconducting circuits are leading candidates for constituting the basic building block of a prospective quantum computer. A common element of all superconducting qubits is the Josephson junction. The nonlinearity of Josephson junctions generates an anharmonic energy spectrum in which the two lowest energy states can be used as the computational basis.[1,2] Over the last decade, there has been a two order of magnitude increase in coherence times of superconducting qubits. This tremendous improvement allowed for demonstration of several major milestones in the pursuit of scalable quantum computing, such as the control and entanglement of multiple qubits.[3,4] Further increases in coherence times will eventually allow for building a fault tolerant quantum computer with a reasonable overhead in terms of error correction, as well as implementing novel quantum simulation schemes by accessing wider experimental parameter ranges.[5] While superconducting qubits embedded in a 3D cavity[6] have shown coherence times in excess of 100 μs,[7] this approach may impose some constraint on the scalability of quantum circuits. Since the Josephson junction itself does not limit qubit coherence,[6] comparably long lifetimes can also be achieved in a planar geometry by careful circuit engineering.

In this paper, we present the design and characterization of a superconducting quantum circuit comprising a concentric transmon qubit,[8] schematically depicted in Fig. 1(a). The two capacitor pads forming the transmon's large shunt capacitance are implemented by a central disk island and a concentrically surrounding ring. The two islands are interconnected by two Josephson junctions forming a gradiometric SQUID. A 50 Ω impedance matched on-chip flux bias line located next to the qubit allows for fast flux tuning of the qubit frequency due to the imposed asymmetry. This guarantees high experimental flexibility and enables full tomographic control. The gradiometric flux loop design reduces the sensitivity to external uniform magnetic fields and thus to external flux noise. For readout and control purposes, we embed the qubit in a microstrip resonator circuit, forming a familiar circuit quantum

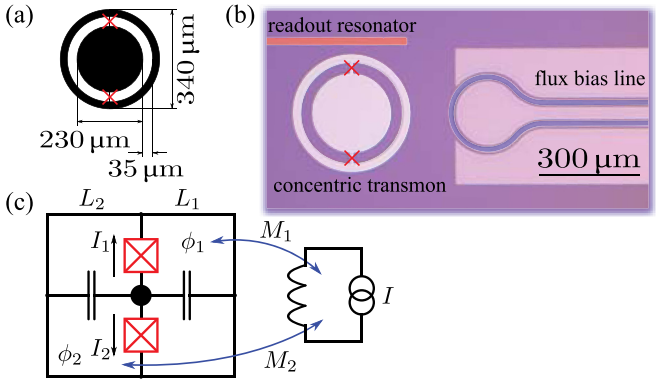

FIG. 1. (a) Geometry of the concentric transmon qubit. Two Josephson junctions (red crosses), located opposite to each other, connect the central island to an outer ring. (b) Optical micrograph of the fabricated sample. The readout resonator (red) capacitively couples to the concentric transmon from above. The on-chip flux bias line (blue) is visible to the right. It is designed in coplanar geometry, having the microwave ground reference in the device plane (bright color). The flux bias line is grounded at one end on the chip. (c) Schematic circuit diagram of the concentric transmon, revealing the gradiometric SQUID architecture. The central part, marked with a black dot, corresponds to the center island of the transmon. Since the mutual inductances to the flux bias line are not equal, $M_1 \neq M_2$, the effective critical current of the SQUID can be tuned.

[a)]Electronic mail: jochen.braumueller@kit.edu.

electrodynamics (cQED) system.[9] The sample is fabricated in hybrid coplanar-microstrip geometry, featuring a ground plane on the backside of the substrate, thus exploiting the increase in mode volume in a microstrip architecture. The circular shape of the transmon features a strongly reduced electric dipole moment due to symmetry and hence a reduction in radiation loss can be expected[10] compared to a regular pad geometry of equal size and electrode spacing. The sample is prepared in a straightforward fabrication process using pure aluminum for the metalization and employing the conventional shadow angle evaporation technique. The best measured relaxation and decoherence times are in the order of $10\,\mu$s.

The schematic circuit diagram of the concentric transmon is depicted in Fig. 1(c). The two Josephson junctions are connecting the central island to the outer ring of the transmon. The islands act as coplanar electrodes[10] giving rise to the total qubit capacitance $C = 81$ fF, including the contribution by the ground plane and coupling capacitances. Considering loop L_1 as the primary transmon loop, the gradiometric dc-SQUID architecture can be recognized. The kinetic inductance of the superconducting aluminum wire can be neglected due to its thickness and the width of the Josephson junction leads. The effective critical current $I_{c,eff}$ of the SQUID is tuned by applying an inhomogeneous magnetic field supplied by the on-chip flux bias line. Due to the gradiometric geometry, the effective critical current $I_{c,eff} = 2I_c|\cos(\pi\Delta\Phi/2\Phi_0)|$ in the primary loop L_1 is $2\Phi_0$-periodic in the flux asymmetry $\Delta\Phi = |\Phi_1 - \Phi_2|$ between the loops. Here, $\Phi_0 = h/2e$ denotes the magnetic flux quantum. We analytically calculate the net mutual inductance to the flux bias line to be 2.3 pH. This yields a flux bias current of 0.9 mA required to induce a Φ_0 in the primary transmon loop.

The fabrication process consists of two subsequent deposition and lithography steps. The feedline, the microstrip resonator, and the flux bias line are structured by optical lithography in a lift-off process of a 50 nm thick aluminum film. After that, the concentric transmon including the Josephson junctions are patterned using electron beam lithography. The Josephson junctions are formed by shadow angle evaporation with electrode film thicknesses of 30 nm and 50 nm, respectively. A 50 nm thick aluminum film is applied on the backside of the intrinsic silicon substrate. Both metalizations on the device side of the chip are deposited by aluminum evaporation at a background chamber pressure of about 3×10^{-8} mbar. A micrograph of the fabricated sample is depicted in Fig. 1(b).

We operate the device at a fundamental qubit transition frequency $\omega_q/2\pi = 6.85$ GHz, away from any flux sweet spot and far detuned from the readout resonator to reduce Purcell dissipation. The Josephson energy $E_J/h = 29$ GHz dominates the charging energy $E_C/h = 0.24$ GHz, yielding $E_J/E_C = 120$. This assures the circuit to be inherently insensitive to charge noise and features an intrinsic self-biasing.[11] The total critical current of both Josephson junctions is 58 nA. Due to its large loop size, the concentric transmon exhibits a notable geometric inductance $L_g = 0.6$ nH, accounting for 10% of the total qubit inductance. As one important consequence, the qubit anharmonicity is not constant with respect to the bias point. For the operation point we extract a relative anharmonicity of 3.4%. Relevant qubit parameters are extracted by fitting an effective system Hamiltonian to spectroscopic data, see supplementary material.[12] By sweeping the flux bias current, we observe a period of 1.7 mA in the qubit transition frequency, confirming the expected $2\Phi_0$-periodicity in good approximation.

Since coherence is relaxation limited, $T_2 \leq 2T_1$, taking effort in increasing T_1 typically results in an increase in T_2. To accomplish this, we engineered the concentric transmon to have a reduced sensitivity to its major loss channels, namely, spontaneous Purcell emission, radiative dipole decay and loss due to surface defect states. Losses due to quasiparticle tunneling processes typically impose a T_1 limitation at around $\sim$1 ms,[13] having no considerable effect on the lifetime of our circuit. Relevant contributions leading to qubit decay are summarized in Table I.

The coupling limited quality factor $Q_L = \omega_r/\kappa$ of the dispersive readout resonator at $\omega_r/2\pi = 8.79$ GHz is 2.1×10^3, close to the design value. The qubit lifetime is potentially Purcell limited by spontaneous emission into modes that are nearby in frequency. Major contributions are the dispersive single-mode decay into the capacitively coupled readout resonator as well as emission into the flux bias line[11,14] due to inductive coupling. The coupling constant $g/2\pi = 55$ MHz between qubit and resonator is extracted from the dispersive shift of the resonator.[15] We calculate a single-mode Purcell limitation induced by the readout resonator of $\Gamma_{1,sm} = \kappa(g/\Delta)^2 = 1/47\,\mu$s at a detuning $\Delta = 1.94$ GHz from the readout resonator. The multi-mode Purcell limitation due to inductive coupling of the qubit to the flux bias line of impedance $Z_0 = 50\,\Omega$ is $\Gamma_{1,ind} = \omega_q^2 M^2/(LZ_0) = 1/32\,\mu$s, with $M = 2.3$ pH being the gradiometric mutual inductance and $L = 6.3$ nH the total qubit inductance. This rather stringent loss channel can be reduced further by decreasing the coupling to the flux bias line. By an analogous approach to account for Purcell decay due to capacitive coupling to the flux bias line ($C_c \sim 0.1$ fF), we calculate $\Gamma_{1,cap} = \omega_q^2 C_c^2 Z_0/C \sim 1/87\,\mu$s. The presented values are approximations and give a rough estimate of the expected Purcell loss. A more stringent analysis would require a full 3D electromagnetic simulation of the circuit and a blackbox quantization.[16]

The coplanar concentric transmon is embedded in a microstrip geometry, where the ground reference on the device side of the substrate is substituted by a backside metalization. The largest fraction of the electric field energy is stored in the substrate, and the field strength at incoherent and weakly coupled defects residing in surface and interface oxides of the sample is reduced due to an increased mode volume. Highest fields in the geometry appear in the gap between the center island and the ring of the concentric transmon

TABLE I. Calculated loss contributions for the concentric transmon qubit. The main contribution $\Gamma_{1,ind}^{-1}$ arises from inductive coupling to the flux bias line, leading to a total Purcell limitation of $\Gamma_{1,P}^{-1} = 16\,\mu$s. The estimated reciprocal sum Γ_{Σ}^{-1} is in good agreement with the measured T_1.

$\Gamma_{1,sm}^{-1}$	Purcell $\Gamma_{1,ind}^{-1}$	$\Gamma_{1,cap}^{-1}$	Defects $\Gamma_{1,TLF}^{-1}$	Radiation $\Gamma_{1,rad}^{-1}$	Reciprocal sum Γ_{Σ}^{-1}
47 μs	32 μs	$\sim$87 μs			
	$\Gamma_{1,P}^{-1} = 16\,\mu$s		$\sim$26 μs	$\gtrsim 100\,\mu$s	8.9 μs

within the substrate. From the vacuum energy of the transmon, we extract a weighted mean electrical field strength $|\vec{E}| = 2.3\,\mathrm{V/m}$ in the surface and interface oxide of an estimated effective volume of $V = 50 \times 10^{-18}\,\mathrm{m}^3$. We assume a maximum defect dipole moment $|\vec{d}_0| = 1.6\,\mathrm{e\AA}$, reported in literature[17,18] as the highest dipole moment observed in Josephson junction barriers and therefore yielding a worst case estimation. We employ a normalized dipole moment distribution[17] $P(p) = A\sqrt{1-p^2}/p$, with relative dipole moment $p = |\vec{d}|/|\vec{d}_0|$. Taking into account a normalized defect probability distribution[19] $P(\omega,\theta) = B\omega^{\alpha}\cos^{\alpha}\theta/\sin\theta$, one can estimate the mean relaxation rate $\Gamma_{1,TLF}$ due to a single incoherent two level fluctuator (TLF) with averaged parameters to be

$$\int_0^{d_0} \mathrm{d}pP(p)\frac{p^2|\vec{E}|^2}{\hbar^2}\int_0^{\omega_{TLF}} \mathrm{d}\omega \int_0^{\pi/2} \mathrm{d}\theta P(\omega,\theta)C(\omega_q). \quad (1)$$

ω denotes the TLF frequency that we integrate to a maximum frequency $\omega_{TLF}/2\pi = 15\,\mathrm{GHz}$, and θ sets the dipole matrix element $\sin\theta$. The spectral density $C(\omega_q) = \sin^2\theta\,\gamma_2/(\gamma_2^2 + (\omega-\omega_q)^2)$ essentially is the Fourier transform of the coupling correlation function,[19] with a TLF dephasing rate $\gamma_2/2\pi = 10\,\mathrm{MHz}$. The averaged rate induced by a single TLF, given in Eq. (1), is multiplied by the number $N = \rho_0 V\hbar\omega_{TLF}$ of defect TLF interacting with the qubit. With a distribution parameter $\alpha = 0.3$ (Ref. 20) and a constructed defect density $\rho_0 = 4\times10^2/\mu\mathrm{m}^3/\mathrm{GHz}$, we compute a T_1 limitation due to the bath of incoherent TLF to be $\Gamma_{1,TLF} \sim 1/26\,\mu\mathrm{s}$. The choice of ρ_0 is consistent with literature[17,21] and is justified by a very good agreement with a loss participation ratio analysis carried out via a finite element simulation, see supplementary material.[12] The calculated decay rate shows a very weak dependence on the employed parameters γ_2, α and integration cutoffs. $\Gamma_{1,TLF}$ imposes a limitation for the best measured T_1 due to the quasi-static bath of incoherent defects. In general, defects in the Josephson junction of the device do not significantly contribute to qubit decay. Due to its small size, the defect density in the Josephson barrier is discretized and therefore highly reduced.[22,23]

As pointed out in Ref. 10, radiative loss becomes apparent for qubits with a large electric dipole moment. Radiative decay is reduced as the dipole of the mirror image, induced by the ground plane of the microstrip geometry, radiates in antiphase, leading to destructive interference. Our circular geometry brings about an additional decrease in radiated power by strongly reducing the electric dipole moment of the qubit. We analyze this by simulating the dissipated power in a conductive plane placed 1.5 mm above our geometry in the medium far field and compare the result to a conventional pad architecture. The internal quality factor of the qubit eigenmode indicates a radiative contribution of $\Gamma_{1,rad}^{-1} \gtrsim 100\,\mu\mathrm{s}$. The radiative dissipation of a comparable qubit in pad geometry exceeds this value by more than an order of magnitude.

The dissipative dynamics of the investigated concentric transmon is depicted in Fig. 2. We excite the qubit by applying a π pulse and measure its state $\langle\hat{\sigma}_z\rangle$ with a strong readout pulse after a varying time delay Δt. The obtained energy

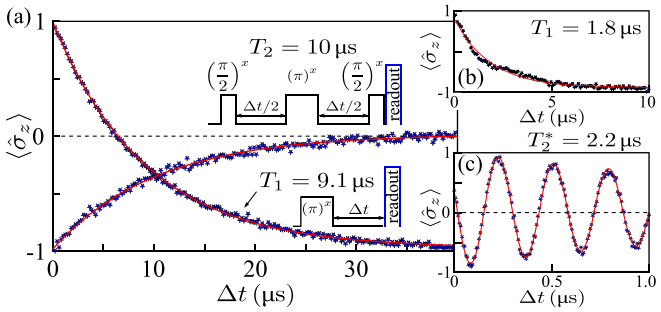

FIG. 2. (a) Measured relaxation time $T_1 = 9.1\,\mu\mathrm{s}$ and dephasing time $T_2 = 10\,\mu\mathrm{s}$ with applied measurement pulse sequences shown in the inset. The operation frequency is $\omega_q/2\pi = 6.85\,\mathrm{GHz}$, corresponding to a detuning of 1.9 GHz below the readout resonator frequency. A Hahn echo pulse is applied in the Ramsey sequence to compensate for low-frequency fluctuations in the qubit transition frequency. (b) and (c) T_1 decay and bare dephasing without echo pulse T_2^* measured at the flux sweet spot at 7.72 GHz. While T_1 is reduced due to Purcell dissipation, T_2^* is comparable to the bare T_2^*, measured far detuned from the sweet spot. The slight deviation from an exponential decay is attributed to excitation leakage.

relaxation time $T_1 = 9.1\,\mu\mathrm{s}$ in Fig. 2(a), lower part, is in good agreement with the estimated T_1 time, see Table I. To verify the presented loss participation ratio analysis, T_1 decay close to the flux sweet spot is shown in Fig. 2(b). The Purcell contribution is calculated to be $4.7\,\mu\mathrm{s}$, reducing the overall dissipation estimate to $3.7\,\mu\mathrm{s}$. The anharmonicity at the flux sweet spot is reduced to 1%, favoring leakage into higher levels and therefore degrading the reliability of the exponential fit. The reduction in T_1 at the sweet spot is not fully understood. A possible explanation is that the presented first order model for estimating Purcell decay is not very accurate for this high geometric inductance transmon. In addition, losses related to the geometric inductance such as quasi particles or magnetic vortices may be more prominent at the flux sweet spot.

In continuous lifetime measurements, we observe temporal fluctuations in T_1 down to about $2\,\mu\mathrm{s}$. We conjecture that this is attributed to discrete TLF dynamics of individual TLF, located in the small oxide volume at the leads to the Josephson junctions, where the electric field strength is enhanced.

The spin echo dephasing time is $T_2 = 10\,\mu\mathrm{s}$, see Fig. 2(a), upper part. Due to the Hahn echo pulse in between the projecting $\pi/2$ pulses, our device is insensitive to low-frequency noise roughly below $1/\Delta t = 25\,\mathrm{kHz}$. A Ramsey $T_2^* \sim 2\,\mu\mathrm{s}$ is measured without echo pulse. It is interesting to note that a rather high T_2 is maintained in spite of the large loop size and while operating the transmon detuned by 1 GHz from its flux sweet spot, where flux noise contributes to pure dephasing. Figure 2(c) shows the dephasing time T_2^* without echo pulse measured at the flux sweet spot. Dephasing, presumably induced in part by local magnetic fluctuators, is reduced due to the vanishing slope of the energy dispersion at the flux sweet spot. In a non-tunable TiN version of the concentric transmon with a single Josephson junction and an opening in the outer ring, we find maximal $T_1 \sim 50\,\mu\mathrm{s}$ and dephasing times up to $T_2^* \sim 60\,\mu\mathrm{s}$ without Hahn echo. Similar coherence times might be

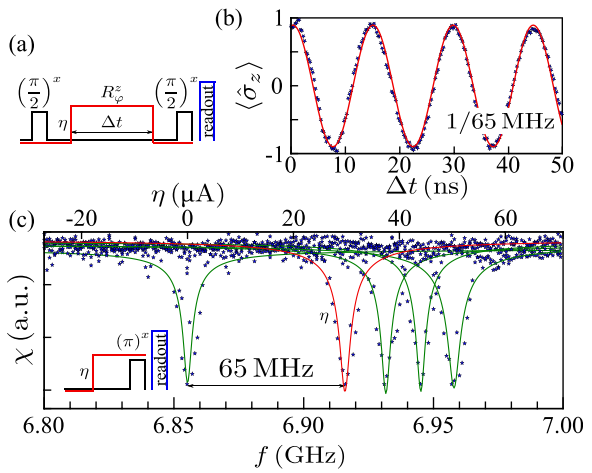

FIG. 3. Demonstration of fast $\hat{Z}$ tunability of the concentric transmon. (a) Pulse sequence applied for calibration. Between two projecting $\pi/2$-pulses we apply a $\hat{Z}$-rotation R_φ^z of amplitude η and length Δt. (b) The expectation value of the qubit state oscillates between its fundamental states $|0\rangle$, $|1\rangle$ with a relative Larmor frequency $\omega_L/2\pi = 65$ MHz for a pulse amplitude of $\eta = 32\,\mu$A. (c) Check measurement of the bare and detuned qubit transition frequency ω_q by exciting with a π-pulse (see inset). The initial frequency is shifted dependent on the amplitude η of the applied current pulse, see different Lorentzian fits. For $\eta = 32\,\mu$A, as applied in (a), we obtain a frequency shift in accordance with the one extracted in (b), see red Lorentzian fit.

achieved for the tunable concentric design by implementing it in a TiN material system. The measured coherence times compare with other planar transmon geometries such as a non-tunable Al based transmon with decreased finger gap size[24] ($T_1 = 9.7\,\mu$s, $T_2^* = 10\,\mu$s) and the cross shaped transmon[21] ($T_1 = 40\,\mu$s, $T_2 = 20\,\mu$s).

Figure 3 demonstrates fast frequency control of the concentric transmon. This is commonly referred to as $\hat{Z}$ control since Pauli's spin operator $\hat{\sigma}_z$ appears in the Hamiltonian representation of the qubit. We record the equatorial precession (see Fig. 3(b)) due to a detuning pulse R_φ^z of amplitude η in between two projective $\pi/2$ pulses. The pulse sequence is given in Fig. 3(a). The pulse amplitude η translates into magnetic flux applied to the flux bias line, see the experimental setup in the supplementary material.[12] In the laboratory frame, this corresponds to a shift in qubit frequency $\Delta f \propto \eta$, which is confirmed in a quasi-spectroscopic measurement by exciting the detuned qubit with a π pulse, see Fig. 3(c). In the frame rotating with the qubit frequency, the R_φ^z pulse induces a change in Larmor frequency, leading to an effective precession in this rotating frame with an angular frequency proportional to the detuning pulse amplitude η. By increasing η, we demonstrated a fast frequency detuning of up to 200 MHz (not shown here). A further increase of the tunability range, requiring pulse shaping, renders our device a valuable tool for a variety of quantum experiments.

We propose the concentric transmon as a suitable candidate to establish a direct inductive $\hat{Z}$ coupling between neighboring qubits. Since the area of the magnetic flux loop is large, the magnetic dipole moment of our qubit is strongly enhanced as compared to conventional transmon designs where it is typically negligible. For two concentric transmon qubits separated by 150 μm, we analytically calculate a maximum mutual inductance $M_{ij} = 31$ pH by applying the double integral Neumann formula.[25] Comparing the ratio $M_{ij}/L \sim 0.5\%$ to the ratio $\beta = C_g/C \sim 10\%$, typical for cQED circuits and corresponding to a 100 MHz coupling, we estimate an inductive $\hat{Z}$ coupling up to $g_z^{ind}/2\pi \sim 5$ MHz. Here, $L = 6.3$ nH is the total qubit inductance and β denotes the ratio of coupling capacitance C_g to total qubit capacitance C. At the given qubit distance, the capacitive coupling is simulated to be in the order of 40 MHz and therefore less than a factor of 10 higher compared to the inductive coupling. To further increase the $\hat{Z}$ coupling, the qubit geometry can be adapted to enhance the mutual inductance. Especially for neighboring qubits being detuned in frequency, the $\hat{Z}$ coupling may dominate the effective transversal capacitive coupling. Since the mutual inductance vanishes completely for adjacent qubits arranged at a relative rotation angle of $\pi/2$ and is reduced by more than an order of magnitude when their Josephson junctions are aligned, the concentric transmon geometry allows for a site-selective $\hat{Z}$ coupling. We consider this scheme as highly promising for the field of quantum simulation, for instance in the context of implementing Ising spin models. Patterning an array of concentric transmon qubits featuring $\hat{X}$ and $\hat{Z}$ coupling along two orthogonal directions while exploiting the strongly reduced off-site inductive interaction may be a route to implement a quantum neural network, which is a powerful tool in quantum computation.[26]

In conclusion, we introduced a planar tunable qubit design based on a superconducting circuit that we call concentric transmon. The observed qubit lifetimes and coherence times are in the order of 10 μs and thereby competitive with conventional transmon geometries. The qubit lifetime is Purcell limited by its readout resonator and the flux bias line. Radiative loss, which is an intrinsic loss channel to the geometry, is demonstrated to be limiting only above $\sim$100 μs, evincing the potential of the reported architecture. A major advantage of our approach is the straightforward fabrication process. We demonstrated full tomographic control of our quantum circuit and discuss the high potential of the presented qubit design for the implementation of a direct site-selective $\hat{Z}$ coupling between neighboring qubits, being a pending quest in quantum simulation.

The authors are grateful for valuable discussions about two-level defects with C. Müller and J. Lisenfeld. We want to thank L. Radtke for assistance in sample fabrication and S. T. Skacel for providing microwave simulations. This work was supported by Deutsche Forschungsgemeinschaft (DFG) within Project No. WE4359/7-1 and through the DFG-Center for Functional Nanostructures National Service Laboratory (CFN-NSL). This work was also supported in part by the Ministry for Education and Science of the Russian Federation Grant No. 11.G34.31.0062 and by NUST MISIS under Contract No. K2-2014-025. J.B. acknowledges financial support by the Helmholtz International Research School for Teratronics (HIRST) and the Landesgraduiertenförderung (LGF) of the federal state Baden-Württemberg.

M.S. conceived the concentric transmon geometry. J.B. designed, fabricated, and measured the tunable concentric transmon circuit. M.S. and M.R.V. designed and fabricated the TiN transmon.

[1]J. Clarke and F. K. Wilhelm, "Superconducting quantum bits," Nature **453**, 1031–1042 (2008).
[2]R. J. Schoelkopf and S. M. Girvin, "Wiring up quantum systems," Nature **451**, 664–669 (2008).
[3]M. Steffen, M. Ansmann, R. C. Bialczak, N. Katz, E. Lucero, R. McDermott, M. Neeley, E. M. Weig, A. N. Cleland, and J. M. Martinis, "Measurement of the entanglement of two superconducting qubits via state tomography," Science **313**, 1423–1425 (2006).
[4]R. Barends, J. Kelly, A. Megrant, A. Veitia, D. Sank, E. Jeffrey, T. C. White, J. Mutus, A. G. Fowler, B. Campbell, Y. Chen, B. Chiaro, A. Dunsworth, C. Neill, P. O'Malley, P. Roushan, A. Vainsencher, J. Wenner, A. N. Korotkov, A. N. Cleland, and J. M. Martinis, "Superconducting quantum circuits at the surface code threshold for fault tolerance," Nature **508**, 500–503 (2014).
[5]G. S. Paraoanu, "Recent progress in quantum simulation using superconducting circuits," J. Low Temp. Phys. **175**, 633–654 (2014).
[6]H. Paik, D. I. Schuster, L. S. Bishop, G. Kirchmair, G. Catelani, A. P. Sears, B. R. Johnson, M. J. Reagor, L. Frunzio, L. I. Glazman, S. M. Girvin, M. H. Devoret, and R. J. Schoelkopf, "Observation of high coherence in Josephson junction qubits measured in a three-dimensional circuit QED architecture," Phys. Rev. Lett. **107**, 240501 (2011).
[7]C. Rigetti, J. M. Gambetta, S. Poletto, B. L. T. Plourde, J. M. Chow, A. D. Córcoles, J. A. Smolin, S. T. Merkel, J. R. Rozen, G. A. K. Keefe, M. B. Rothwell, M. B. Ketchen, and M. Steffen, "Superconducting qubit in a waveguide cavity with a coherence time approaching 0.1 ms," Phys. Rev. B **86**, 100506 (2012).
[8]M. Sandberg, E. Knill, E. Kapit, M. R. Vissers, and D. P. Pappas, "Efficient quantum state transfer in an engineered chain of quantum bits," Quantum Inf. Process. (published online 2015).
[9]A. Wallraff, D. I. Schuster, A. Blais, L. Frunzio, R.-S. Huang, J. Majer, S. Kumar, S. M. Girvin, and R. J. Schoelkopf, "Strong coupling of a single photon to a superconducting qubit using circuit quantum electrodynamics," Nature **431**, 162–167 (2004).
[10]M. Sandberg, M. R. Vissers, T. A. Ohki, J. Gao, J. Aumentado, M. Weides, and D. P. Pappas, "Radiation-suppressed superconducting quantum bit in a planar geometry," Appl. Phys. Lett. **102**, 072601 (2013).
[11]J. Koch, T. M. Yu, J. Gambetta, A. A. Houck, D. I. Schuster, J. Majer, A. Blais, M. H. Devoret, S. M. Girvin, and R. J. Schoelkopf, "Charge-insensitive qubit design derived from the cooper pair box," Phys. Rev. A **76**, 042319 (2007).
[12]See supplementary material at http://dx.doi.org/10.1063/1.4940230 for a description of the experimental setup, the extraction of qubit parameters via an effective system Hamiltonian and a finite element simulation of dielectric loss.
[13]D. Ristè, C. C. Bultink, M. J. Tiggelman, R. N. Schouten, K. W. Lehnert, and L. DiCarlo, "Millisecond charge-parity fluctuations and induced decoherence in a superconducting transmon qubit," Nat. Commun. **4**, 1913 (2013).
[14]A. A. Houck, J. A. Schreier, B. R. Johnson, J. M. Chow, J. Koch, J. M. Gambetta, D. I. Schuster, L. Frunzio, M. H. Devoret, S. M. Girvin, and R. J. Schoelkopf, "Controlling the spontaneous emission of a superconducting transmon qubit," Phys. Rev. Lett. **101**, 080502 (2008).
[15]J. Braumüller, J. Cramer, S. Schlör, H. Rotzinger, L. Radtke, A. Lukashenko, P. Yang, S. T. Skacel, S. Probst, M. Marthaler, L. Guo, A. V. Ustinov, and M. Weides, "Multiphoton dressing of an anharmonic superconducting many-level quantum circuit," Phys. Rev. B **91**, 054523 (2015).
[16]F. Solgun, D. W. Abraham, and D. P. DiVincenzo, "Blackbox quantization of superconducting circuits using exact impedance synthesis," Phys. Rev. B **90**, 134504 (2014).
[17]J. M. Martinis, K. B. Cooper, R. McDermott, M. Steffen, M. Ansmann, K. D. Osborn, K. Cicak, S. Oh, D. P. Pappas, R. W. Simmonds, and C. Y. Clare, "Decoherence in Josephson qubits from dielectric loss," Phys. Rev. Lett. **95**, 210503 (2005).
[18]J. H. Cole, C. Müller, P. Bushev, G. J. Grabovskij, J. Lisenfeld, A. Lukashenko, A. V. Ustinov, and A. Shnirman, "Quantitative evaluation of defect-models in superconducting phase qubits," Appl. Phys. Lett. **97**, 252501 (2010).
[19]C. Müller, J. Lisenfeld, A. Shnirman, and S. Poletto, "Interacting two-level defects as sources of fluctuating high-frequency noise in superconducting circuits," Phys. Rev. B **92**, 035442 (2015).
[20]L. Faoro and L. B. Ioffe, "Interacting tunneling model for two-level systems in amorphous materials and its predictions for their dephasing and noise in superconducting microresonators," Phys. Rev. B **91**, 014201 (2015).
[21]R. Barends, J. Kelly, A. Megrant, D. Sank, E. Jeffrey, Y. Chen, Y. Yin, B. Chiaro, J. Mutus, C. Neill, P. O'Malley, P. Roushan, J. Wenner, T. White, A. N. Cleland, and J. M. Martinis, "Coherent Josephson qubit suitable for scalable quantum integrated circuits," Phys. Rev. Lett. **111**, 080502 (2013).
[22]M. Weides, R. C. Bialczak, M. Lenander, E. Lucero, M. Mariantoni, M. Neeley, A. D. O'Connell, D. Sank, H. Wang, J. Wenner, Y. Yamamoto, Y. Yin, A. N. Cleland, and J. M. Martinis, "Phase qubits fabricated with trilayer junctions," Supercond. Sci. Technol. **24**, 055005 (2011).
[23]M. P. Weides, J. S. Kline, M. R. Vissers, M. O. Sandberg, D. S. Wisbey, B. R. Johnson, T. A. Ohki, and D. P. Pappas, "Coherence in a transmon qubit with epitaxial tunnel junctions," Appl. Phys. Lett. **99**, 262502 (2011).
[24]J. M. Chow, J. M. Gambetta, A. D. Córcoles, S. T. Merkel, J. A. Smolin, C. Rigetti, S. Poletto, G. A. Keefe, M. B. Rothwell, J. R. Rozen, M. B. Ketchen, and M. Steffen, "Universal quantum gate set approaching fault-tolerant thresholds with superconducting qubits," Phys. Rev. Lett. **109**, 060501 (2012).
[25]J. Jackson, *Classical Electrodynamics* (John Wiley & Sons, Inc., New York, 1962).
[26]M. Schuld, I. Sinayskiy, and F. Petruccione, "The quest for a quantum neural network," Quantum Inf. Process. **13**, 2567–2586 (2014).